



**HAL**  
open science

# Characterizing Mars's Magnetotail Topology With Respect to the Upstream Interplanetary Magnetic Fields

Shaosui Xu, David L. Mitchell, Tristan Weber, David A. Brain, Janet G. Luhmann, Chuanfei Dong, Shannon M. Curry, Yingjuan Ma, Gina A. Dibraccio, Jasper Halekas, et al.

## ► To cite this version:

Shaosui Xu, David L. Mitchell, Tristan Weber, David A. Brain, Janet G. Luhmann, et al.. Characterizing Mars's Magnetotail Topology With Respect to the Upstream Interplanetary Magnetic Fields. *Journal of Geophysical Research Space Physics*, 2020, 125, 10.1029/2019JA027755 . insu-03673163

**HAL Id: insu-03673163**

**<https://insu.hal.science/insu-03673163>**

Submitted on 20 May 2022

**HAL** is a multi-disciplinary open access archive for the deposit and dissemination of scientific research documents, whether they are published or not. The documents may come from teaching and research institutions in France or abroad, or from public or private research centers.

L'archive ouverte pluridisciplinaire **HAL**, est destinée au dépôt et à la diffusion de documents scientifiques de niveau recherche, publiés ou non, émanant des établissements d'enseignement et de recherche français ou étrangers, des laboratoires publics ou privés.

Copyright

# JGR Space Physics

## RESEARCH ARTICLE

10.1029/2019JA027755

### Key Points:

- This study provides a detailed mapping of tail magnetic topology at Mars, which is dominated by draped and open magnetic field lines
- Both the MHD model and data show significant changes in Martian tail topology with respect to east/west IMF
- It implies that Mars's crustal fields have a global effect on the magnetosphere configuration, supporting the picture of a hybrid magnetotail

### Supporting Information:

- Supporting Information S1

### Correspondence to:

S. Xu,  
shaosui.xu@ssl.berkeley.edu

### Citation:










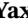


Xu, S., Mitchell, D. L., Weber, T., Brain, D. A., Luhmann, J. G., Dong, C., et al. (2020). Characterizing Mars's magnetotail topology with respect to the upstream interplanetary magnetic fields. *Journal of Geophysical Research: Space Physics*, 125, e2019JA027755. <https://doi.org/10.1029/2019JA027755>

Received 24 DEC 2019

Accepted 7 FEB 2020

Accepted article online 19 FEB 2020

## Characterizing Mars's Magnetotail Topology With Respect to the Upstream Interplanetary Magnetic Fields

Shaosui Xu<sup>1</sup> , David L. Mitchell<sup>1</sup> , Tristan Weber<sup>2</sup> , David A. Brain<sup>2</sup> , Janet G. Luhmann<sup>1</sup> , Chuanfei Dong<sup>3</sup> , Shannon M. Curry<sup>1</sup> , Yingjuan Ma<sup>4</sup> , Gina A. DiBraccio<sup>5</sup> , Jasper Halekas<sup>6</sup> , Yaxue Dong<sup>2</sup> , and Christian Mazelle<sup>7</sup> 

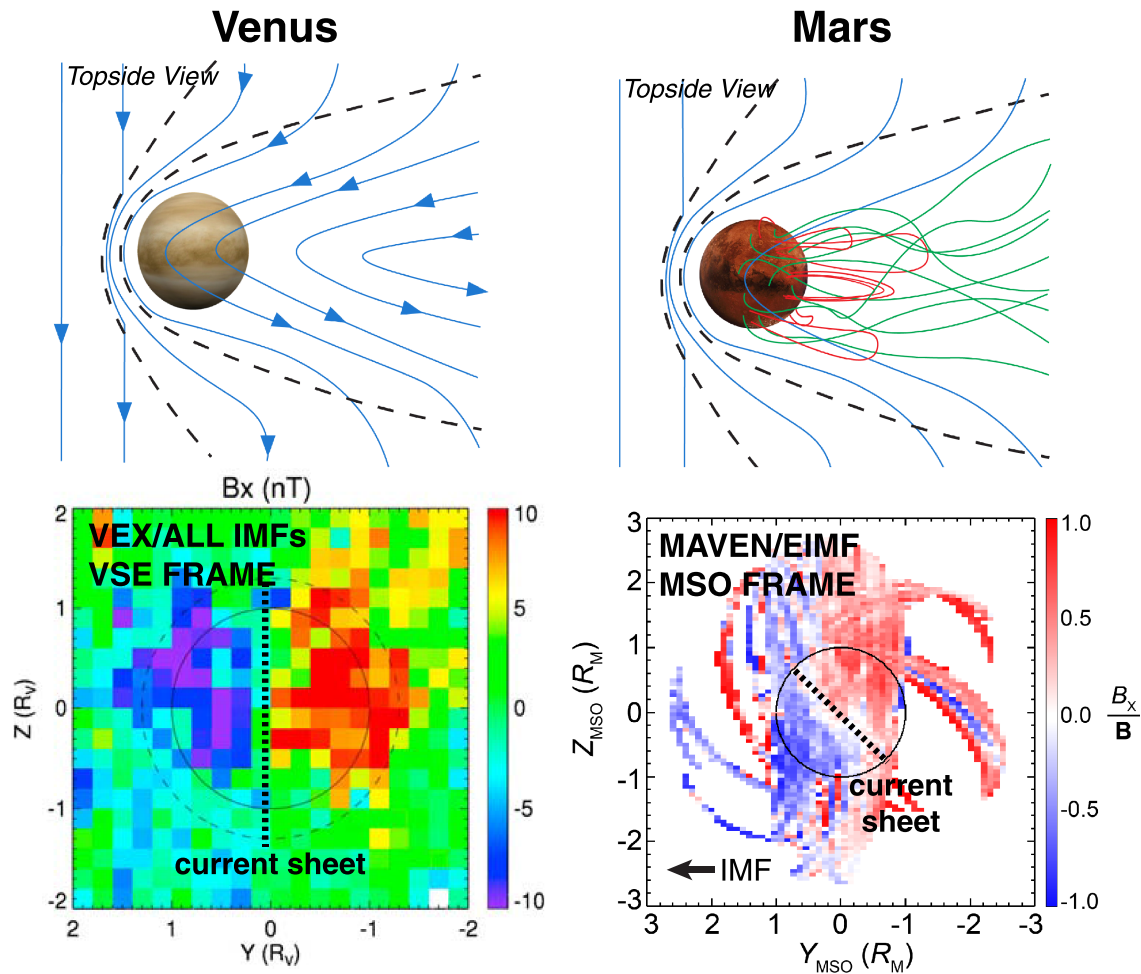
<sup>1</sup>Space Sciences Laboratory, University of California, Berkeley, Berkeley, CA, USA, <sup>2</sup>Laboratory for Atmospheric and Space Physics, University of Colorado Boulder, Boulder, CO, USA, <sup>3</sup>Department of Astrophysical Sciences and Princeton Plasma Physics Laboratory, Princeton University, Princeton, NJ, USA, <sup>4</sup>Department of Earth and Space Sciences, University of California, Los Angeles, Los Angeles, CA, USA, <sup>5</sup>NASA Goddard Space Flight Center, Greenbelt, MD, USA, <sup>6</sup>Department of Physics and Astronomy, University of Iowa, Iowa City, IA, USA, <sup>7</sup>IRAP, CNRS-University of Toulouse-UPS-CNES, Toulouse, France

**Abstract** The canonical picture of the magnetotail of unmagnetized planets consists of draped interplanetary magnetic fields (IMFs) forming opposite-directed lobes, separated by the current sheet. DiBraccio et al. (2018, <https://doi.org/10.1029/2018GL077251>) showed that Mars's magnetotail has a twist departing from this picture. Magnetohydrodynamic (MHD) results suggest that the asymmetry in how open field lines connected to the planet populate the tail causes the apparent twist. To validate this interpretation, we compare the tail topology determined from MHD simulations to that inferred from data collected by the Mars Atmosphere and Volatile Evolution (MAVEN) spacecraft, in particular, how each topology responds to the upstream IMF orientation. The occurrence rates for open topology from both data and MHD vary with IMF polarities in a similar fashion as the tail twisting. This suggests that Mars's crustal fields have a global effect on the magnetosphere configuration, supporting the picture of a “hybrid” magnetotail that is partly induced/draped and partly intrinsic/planetary in origin.

**Plain Language Summary** The interaction of the solar wind with unmagnetized planets, such as Venus, results in an induced magnetotail, which is formed by the interplanetary magnetic field lines draping around the planet, forming opposite-directed lobes. Mars is similar to Venus in many aspects and was thought to have a similar tail configuration. A recent study, however, shows that Mars has a twist in its tail lobes and that modeling results suggest this twist is caused by the effects of its crustal magnetism. In this study, we use the superthermal electron measurements from MAVEN to infer the magnetotail topology resulting from the interaction between the solar magnetic fields and Mars's crustal fields, which is compared with the global magnetohydrodynamic model topology. Our results support the hypothesis that magnetic reconnection between crustal magnetic sources and the solar wind is responsible for the observed twist in Mars's tail lobes.

## 1. Introduction

Venus and Mars both lack an intrinsic global dipole magnetic field but have a significant ionosphere mainly produced by solar extreme ultraviolet photons ionizing the neutral atmosphere, and thus share many similarities in terms of their interaction with the solar wind. Both have an induced magnetosphere formed with the upstream interplanetary magnetic field (IMF) being piled up and draped around the planet. A prominent difference between these two planets is that Mars possesses localized strong crustal magnetic fields (e.g., Acuna et al., 1999; Connerney et al., 2005) that contribute to and modify its induced magnetosphere features on a global scale (e.g., Brain et al., 2007) while Venus has a negligible intrinsic dipole magnetic field at the current epoch (e.g., Phillips & Russell, 1987). As a result, Venus's induced magnetotail consists of two magnetic lobes with oppositely directed magnetic fields formed by draped IMF, separated by a current sheet perpendicular to the plane of the IMF and the solar wind flow (e.g., Luhmann, 1986; McComas et al., 1986; Saunders & Russell, 1986; Zhang et al., 2010), as illustrated in the left column of Figure 1. Note that



**Figure 1.** The comparison of the Venus's (left column) and Mars's magnetotails (right column). The top two panels are schematics of the tail configuration and magnetic topologies and the bottom two panels are the averaged  $B_x$  in the tail from measurements by Venus Express and MAVEN, (adopted from Figure 2 of Zhang et al., 2010 and Figure 2 of DiBraccio et al., 2018), respectively. The dotted black lines in the bottom panels indicate the current sheet that separates the two lobes. The lower left panel is for all IMF directions under the Venus Solar Electric coordinates (VSE) such that the  $X$  axis is antiparallel to the solar wind flow, the  $Z$  axis aligned with the convection electric field ( $\mathbf{E}_{\text{conv}} = -\mathbf{V} \times \mathbf{B}$ ), and the  $Y$  axis completing the right-handed system. The lower right panel is in the Mars-centered Solar Orbital (MSO) frame for east IMFs only. In the MSO frame, the  $X$  axis points from the center of Mars to the Sun, the  $Z$  axis points to the north pole of Mars's elliptical orbit plane, and the  $Y$  axis completes the right-handed system.

the bottom two panels in Figure 1 cannot be used for a direct comparison as they are under different IMF conditions and in different coordinate frames. We use them here to illustrate the typical tail configurations of Venus and Mars.

In contrast, Mars's magnetotail departs from this canonical induced-tail picture, having an apparent inter-lobe current sheet twist away from the expected  $\pm \mathbf{E}_{\text{conv}}$  location, as reported by DiBraccio et al. (2018), also shown in the right column of Figure 1. This twist also varies depending on the IMF sector (hereafter referred as east and west, corresponding to Parker spiral fields pointing away from and toward the Sun, as well as  $B_y > 0$  and  $B_y < 0$ , respectively), suggesting that Mars's crustal magnetic fields play a role. DiBraccio et al. (2018) further compared the tail configuration from magnetohydrodynamics (MHD) with or without crustal magnetic fields included and revealed that the tail twist was indeed attributed to the inclusion of crustal magnetic fields. The tail twist controlled by the  $Y$  component of IMF is a well-known phenomenon of the Earth's magnetotail, where magnetopause reconnection causes an asymmetric addition of open magnetic flux to the tail lobes (e.g., Cowley, 1981). DiBraccio et al. (2018) proposed that Mars's magnetotail is part of a hybrid magnetosphere, consisting of a global intrinsic dipole field (from the low-order dipole term of the crustal magnetism) contribution surrounded by induced/draped fields (Dubinin et al., 1980, 1994).

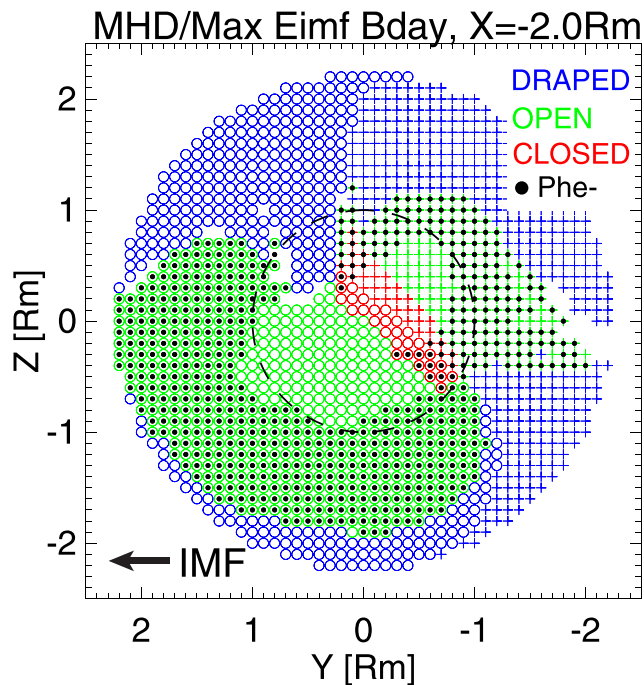
Mars's crustal magnetic fields can magnetically reconnect with the IMF (e.g., Harada et al., 2017, 2018), giving rise to complex and dynamic magnetic topologies (e.g., Brain et al., 2007; Lillis & Brain, 2013; Weber et al., 2019; Xu et al., 2018a, 2019a). Magnetic topology consists of closed (both of the footpoints of a magnetic field line connected to the planet), open (one footpoint of a field line connected to the planet and the other to the solar wind), and draped (both of the footpoints of a field line connected back to the solar wind). Mars's magnetotail consists of various magnetic topologies, instead of simply draped like Venus, as reported by previous studies. Nightside tail topology at low altitudes has been studied in detail with Mars Global Surveyor data (Brain et al., 2007) and MAVEN data (Weber et al., 2017). Photoelectrons have been observed in the tail by both the Mars Express (MEx) spacecraft (Coates et al., 2011; Frahm et al., 2006, 2010) and MAVEN (Xu et al., 2016a, 2017a, 2017b), interpreted as magnetic connectivity to the dayside ionosphere through open field lines (Liemohn et al., 2006) or closed field lines (Xu et al., 2016a, 2017b). Luhmann et al. (2015a) analyzed magnetic topology from MHD simulations and found that a significant portion of Mars's magnetotail is populated with open field lines.

The magnetotail topology is also important for characterizing electron precipitation (e.g., Adams et al., 2018; Fillingim et al., 2007; Lillis et al., 2011; Němec et al., 2010; Shane et al., 2016) and low-energy ion escape (e.g., Dubinin et al., 2017; Fränz et al., 2015; Inui et al., 2018). Solar wind electrons can precipitate along open field lines, and ionospheric photoelectrons along cross-terminator closed field lines onto the (nightside) atmosphere, causing ionization, and auroral emission. Meanwhile, low-energy ions can escape along open field lines (e.g., Ergun et al., 2015; Jakosky et al., 2018), partly driven by ambipolar electric fields (e.g., Akbari et al., 2019; Collinson et al., 2015; Ergun et al., 2016; Xu et al., 2018b), and on draped field lines, mainly accelerated by the  $\mathbf{J} \times \mathbf{B}$  force and/or the convection electric field (e.g., Cravens et al., 2017; Dong et al., 2014; Fang et al., 2008; Halekas et al., 2017a). More general properties of the Martian magnetotail are discussed in several review papers (Bertucci et al., 2011; Dubinin & Fraenz, 2015; Liemohn & Xu, 2018; Nagy et al., 2004).

DiBaccio et al. (2018) advocated for the key role of the crustal fields in introducing the twist to Mars's magnetotail with MAVEN magnetic field data and modeling efforts. The interaction of crustal fields and the IMF results in complex magnetic topology close to Mars and mainly open and draped fields in the tail with a pattern that differs significantly for the two main IMF orientations. To further validate the picture of a hybrid Martian magnetotail, we compare the actual tail topology determined from the MHD simulations with topology inferred from the MAVEN superthermal electron data, in particular, how each magnetic topology varies with respect to the upstream IMF polarity. The results of this study on the detailed characterization of the tail topology are also important for understanding the energy and particle exchange between Mars's ionosphere and the solar wind.

## 2. Methodology

To infer magnetic topology from MAVEN data, we utilize a new technique developed by Xu et al. (2019b) that combines superthermal electrons' energy and pitch angle distributions. This technique mainly relies on three basic principles: (1) the presence of photoelectrons in one or both field-aligned directions indicates that the magnetic field line has one or both footpoint(s) embedded in the *dayside* ionosphere at the superthermal electron exobase ( $\sim 160$  km, Xu et al., 2016b); (2) the presence of loss cones in one or both field-aligned directions indicates that the magnetic field line has one or both footpoint(s) embedded in the collisional atmosphere; (3) the presence of superthermal electron voids indicates that both footpoints of the magnetic field line are connected to the *nightside* atmosphere (Mitchell et al., 2001; Steckiewicz et al., 2015). Magnetic topology is determined based on where each end of the field line is inferred to connect. One caveat of inferring magnetic topology from electrons is that we can only determine field lines' connectivity to the ionosphere but not to the planet's surface so that deeply draped field lines can be identified as "open" topology. Photoelectrons can be identified automatically with a shape parameter (Xu et al., 2017a), loss cones with a pitch angle distribution (PAD) score (Weber et al., 2017), and electron voids by the electron flux level. The detailed description of how to combine all these aspects to infer magnetic topology is provided in Xu et al. (2019b). In this study, we analyze magnetic topology from December 2014 to September 2018, based on the superthermal electron measurements by the Solar Wind Electron Analyzer (SWEA) instrument (Mitchell et al., 2016) and magnetic field vector measurements by the magnetometer (MAG) instrument (Connerney et al., 2015) onboard MAVEN.



**Figure 2.** Magnetic topology from MHD at  $X_{\text{MSO}} = -2 R_M$  for an east upstream IMF and strong crustal fields located on the dayside ( $\text{SSL} = 180^\circ$ ), blue for draped, green for open, and red for closed, with black dots indicating field lines connected back to dayside. Circles are for  $B_x < 0$  and “+” for  $B_x > 0$ . The blank spots within  $2.3 R_M$  are when field line tracing is not successful.

When the MAVEN orbit samples the upstream solar wind, we obtain the IMF clock angle,  $\tan^{-1}(B_z/B_y)$  in the MSO frame, directly from MAG measurements in that region (Halekas et al., 2015, 2017b). Otherwise, we use a proxy based on MAG measurements in the sheath (Dong et al., 2019). Thus, each pass through the tail has IMF clock angle estimates both before and after. We then assign each inferred magnetic topology within the magnetosphere with an upstream IMF clock angle by interpolating between the inbound and outbound values.

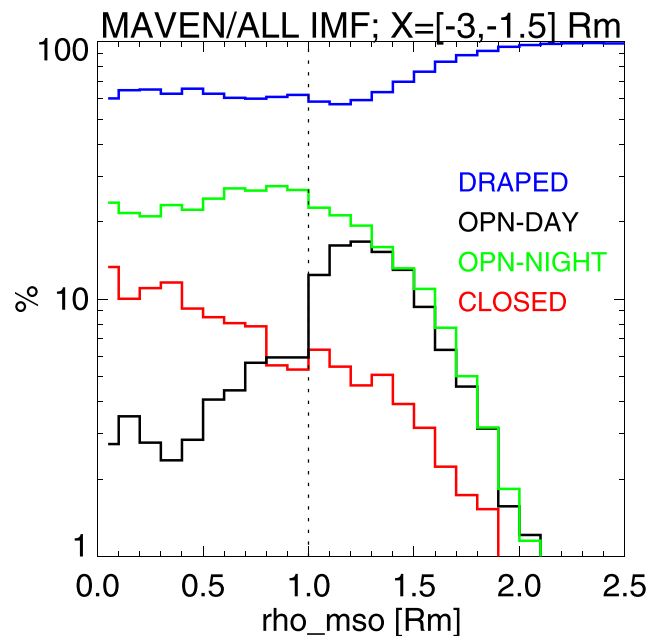
We determine the occurrence rate of the model magnetic topology from 16 steady-state simulations with the multispecies 3-D MHD model (Ma et al., 2002, 2004). Nominal Parker spiral IMFs and a nominal solar wind proton density ( $4 \text{ cm}^{-3}$ ) and speed (400 km/s) with the fall equinox condition are used. Eight simulations are generated for the east IMF ( $B_y > 0$ ) and eight for the west IMF ( $B_y < 0$ ) in the MSO frame. For each IMF direction, the eight simulations consist of the neutral atmospheres and ionization frequencies for the solar maximum and minimum conditions as well as four subsolar longitudes (SSL) for when the southern strong crustal magnetic fields are located on the dayside ( $\text{SSL} = 180^\circ$ ), dawn ( $\text{SSL} = 90^\circ$ ), dusk ( $\text{SSL} = 270^\circ$ ), and nightside ( $\text{SSL} = 0^\circ$ ). For each simulation, magnetic field line tracing starts from a grid of points in the Y-Z plane at  $X = -1.5 R_M$ ,  $X = -2 R_M$ , and  $X = -2.5 R_M$ , separately. Magnetic topology for each field line is determined by its intersection with one or both of two Mars-centered spheres: an inner sphere at 150 km altitude and an outer sphere at a radial distance of  $5.5 R_M$ , where  $R_M$  is the Mars radius. The occurrence rate is calculated as the fraction of each magnetic topology type in the respective tail grid from three X cuts for the eight simulations in each IMF sector; that is, each grid point has 24 samples of topology. We note that the models provide steady-state “snapshots” of the Mars field topology, which in reality is constantly changing as Mars rotates (Ma et al., 2014).

In this study, we focus on qualitative comparison on the gross features of magnetic topology from MAVEN data and MHD, as there are caveats for each data set. For the data, SWEA has an angular resolution of  $\sim 20^\circ$ , which might be insufficient to detect small loss/source cones, expected to be smaller than  $10^\circ$  over strongly magnetized regions of the crust. Therefore, our method might misidentify open field lines connected to strong crustal fields as draped. In addition, the IMF clock angle might vary between the time it is measured upstream of the bow shock (or by proxy in the magneosheath) and the time we infer magnetic topology in the tail. The IMF clock angle proxy determined in the sheath also has an uncertainty of a few tens of degrees (Dong et al., 2019). For the models, the multispecies MHD simulation relies on numerical diffusion as a substitute for magnetic diffusion to enable magnetic reconnection. It is not known how well this approach approximates the physics of magnetic reconnection. Furthermore, magnetic topology is obtained by tracing the magnetic field vector over large distances, which can accumulate error. Lastly, the occurrence rate from MHD is based on only eight steady-state simulations for each IMF polarity, which might not accurately reflect the actual sampling of data over different seasons and continuously rotating crustal field orientations. Despite these limitations, the model results and data results in this study show reasonable qualitative agreements, which suggests that the MHD simulations can provide useful physical insight into the magnetic topology of the tail.

### 3. Results

#### 3.1. Detailed Magnetic Topology From MHD and MAVEN

As illustrated in the lower right panel of Figure 1, as well as Figure 2 of DiBraccio et al. (2018), Mars’s magnetotail has a twist in its lobes and current sheet. MHD results show that this twist also has topological signatures. We take the tail topology from MHD at  $X_{\text{MSO}} = -2 R_M$  under the east IMF condition as an example, shown in Figure 2. The tail field topology from MHD consists of draped field lines (blue) in the outermost layer, surrounding mostly open field lines connected to the dayside (green with black dots overplotted), and



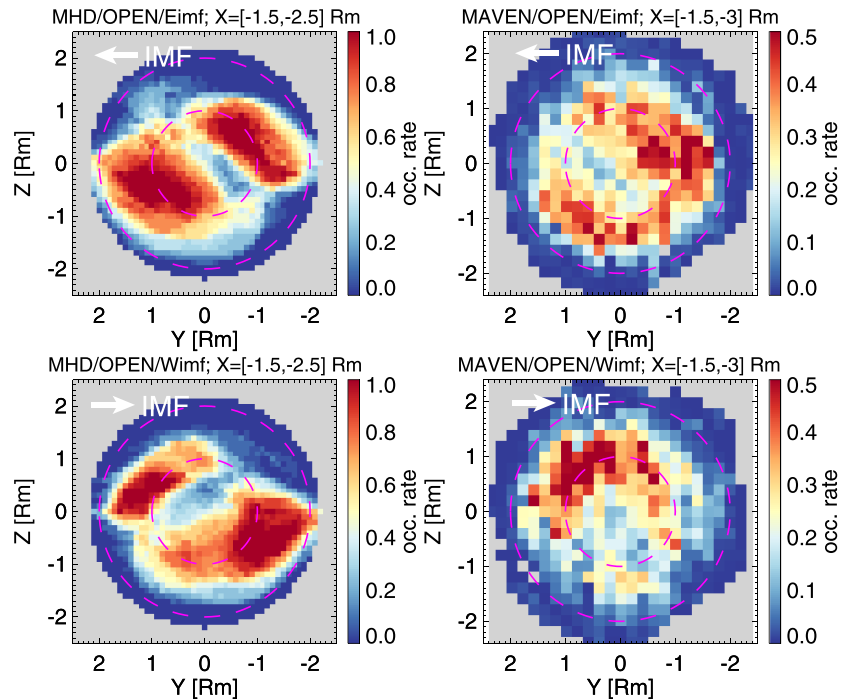
**Figure 3.** The cylindrical averaged occurrence rates of magnetic topologies in the tail ( $X_{\text{MSO}} = [-3, -1.5] R_M$ ) from MAVEN data for all IMFs as a function of  $\rho_{\text{MSO}} = \sqrt{Y_{\text{MSO}}^2 + Z_{\text{MSO}}^2}$ , blue for draped, black for open-to-day, green for open-to-night, and red for closed.

then open field lines connected to the nightside (green). There is also a central region of closed field lines (red) whose size varies with down-tail distance. The twist of the tail current sheet is manifested in mainly the closed and open topologies, suggesting the importance of magnetic topology in imposing the twist. A similar trend is found in the other 15 MHD simulations, with a case for the west IMF shown in Figure S1b in the supporting information.

Magnetic topology inferred from MAVEN data (Figure 3) shows a systematic variation in the dominant topology with distance from the MSO  $X$  axis (tail center line). This is qualitatively similar to the MHD results, as shown for one of the 16 simulations in Figure 2. The cylindrically averaged occurrence rates of magnetic topologies for all IMFs are calculated and shown, because they are roughly cylindrically symmetric (as shown in Figures S1c–S1f in the supporting information). The data results show that draped fields occur over 80% of the time for  $\rho > 1.5 R_M$  (note the log scale for percentage), open-to-day fields are mostly concentrated at  $1 < \rho < 1.5 R_M$ , open-to-night fields occur most frequently within the optical shadow, and the occurrence rates for closed fields peak at 10% at the center. This ordering of where each topology occurs most frequently agree with MHD results.

### 3.2. Data-Model Comparison for Different IMF Polarities

To examine how the IMF polarity affects the tail topology for both MHD and the data, we compare occurrence rates for the east and west IMF separately. The occurrence rates from the data have been averaged over all planetary rotations and over a range of extreme ultraviolet flux and solar wind conditions. To better capture the twist, we limit our analysis to when the IMF is within  $30^\circ$  of the  $X_{\text{MSO}}-Y_{\text{MSO}}$  plane. To approximate this with the MHD simulations, we average the topology in two groups of eight models (four SSLs  $\times$  2 solar conditions for east and west IMF separately) at three  $X$  distances ( $X = -1.5, -2, \text{ and } -2.5 R_M$ ). The comparison is shown in Figure 4. The color range is 0 to 1 for MHD results (left column) but 0 to 0.5 for open field lines for MAVEN results (right column), as the occurrence rates from MHD are roughly twice that of MAVEN data. We use different color ranges to highlight relative variations in the occurrence rates. Because of the aforementioned caveats, the disagreement in the absolute occurrence rate is not unexpected. The high occurrence rate of open topology from the model suggests an artificially high reconnection rate (from numerical diffusion), which leads to more field lines connected to crustal sources. This serves as a reminder to focus on qualitative comparisons between the simulations and the data.

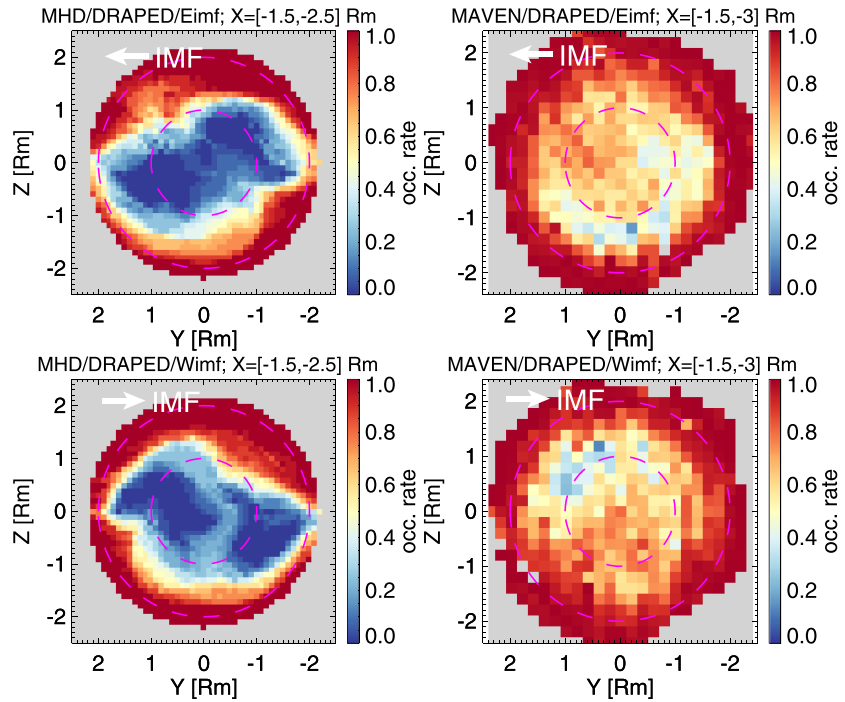


**Figure 4.** Model-data comparison for open topology for east (top row) and west IMF (bottom row). The left column shows the occurrence rates from MHD at  $X_{\text{MSO}} = [-1.5, -2.5] R_M$ , calculated from eight simulations (four SSLs and two solar conditions) separately for each and west IMFs, and right from MAVEN data for  $X_{\text{MSO}} = [-1.5, -3] R_M$ . Note that the color ranges for the occurrence rates from MHD (left column) and data (right column) are different to highlight features.

Despite differences in the overall occurrence rates from the model and data, the patterns of the occurrence rates and their variation with respect to IMF polarities share similarities. For east IMF (top row), the open topology occurs most frequently in the  $+Z/ -Y$  and  $-Z/ +Y$  quadrants in both simulations and data, in agreement with the orientation of the current sheet for this IMF direction as shown in Figure 2 of DiBraccio et al. (2018). For west IMF (bottom row), open topology occurs most frequently in the  $+Z/ +Y$  quadrant in both simulations and data, but only simulations show a significant region of open topology in the  $-Z/ -Y$  quadrant. Again, these topological results are in agreement with a  $\sim 90^\circ$  rotation of the current sheet about the  $X$  axis when the IMF polarity changes from east to west (DiBraccio et al., 2018).

The occurrence rates for draped topology from MHD and data are shown in Figure 5, separated for east and west upstream IMFs. The pattern of low occurrence rates from MHD (left column in Figure 5) shifts significantly for the east and west IMF, corresponding to the variation in open topology in the left column in Figure 4. A corresponding variation in draped topology from the MAVEN data (right column in Figure 5) to the open topology (right column in Figure 4) is seen as well, low occurrence rates in the  $+Y/ +Z$  and  $-Y/ -Z$  quadrants for east IMFs and in the  $-Y/ +Z$  quadrants for west IMFs. Quantitatively, the occurrence rate for draped topology in the data is mostly above 50% whereas the open topology shown in Figure 4 has an occurrence rate below 50%. In contrast, the probability for draped topology from MHD reaches down to nearly 0 within the two tail lobes, where open topology prevails instead. Furthermore, MHD predicts a higher occurrence rate of closed field lines near the current sheet (Figure 2), which is not present in the data.

In summary, the discrepancies between results from the MAVEN data and MHD modeling include the following: (a) a factor of 2 difference in the maximum occurrence rates for the open topology, (b) occurrence rates in the  $-Y/ -Z$  quadrant, and (c) occurrence rates for closed field lines. These discrepancies can probably be explained by some combination of the caveats listed in the section 2. Despite these discrepancies, the pattern of open topology in both simulations and data respond similarly to a reversal of the upstream IMF polarity, probably because the magnetic reconnection patterns of the crustal magnetic fields with east and west IMFs are different.

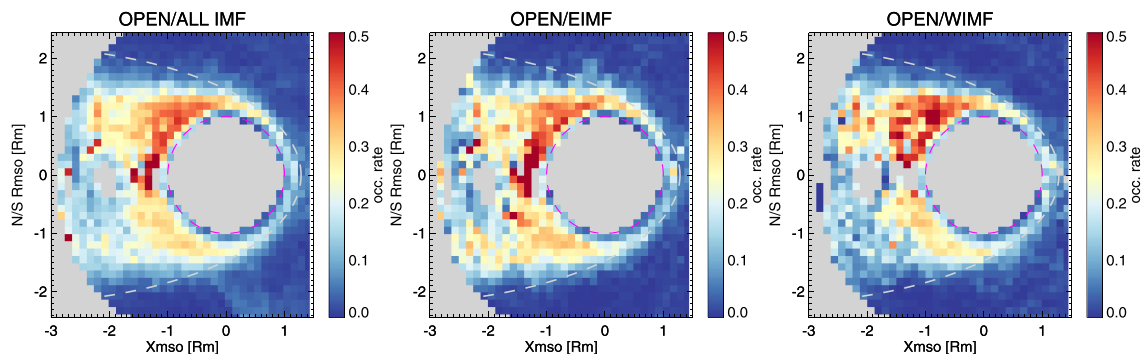


**Figure 5.** Model-data comparison for draped topology for east (top row) and west IMF (bottom row). The same format as Figure 4 but for draped topology. The left column shows the occurrence rates from MHD at  $X_{\text{MSO}} = [-1.5, -2.5] R_M$  and right from MAVEN data  $X_{\text{MSO}} = [-1.5, -3] R_M$ .

### 3.3. Open Topology in the Tail

The results above suggest that the presence of a high occurrence rate of open topology significantly impacts the Martian magnetotail configuration. It also has important implications for characterizing cold ion outflow and electron precipitation. In Figure 6, we show the occurrence rates for the open topology in the  $X_{\text{MSO}}-R_{\text{MSO}}$  projection, where  $R_{\text{MSO}} = \frac{Z_{\text{MSO}}}{|Z_{\text{MSO}}|} \sqrt{Y_{\text{MSO}}^2 + Z_{\text{MSO}}^2}$ .

Overall, the occurrence rate of the open topology mostly ranges from 20% to 50% on the nightside, decreasing with distance down the tail (Figure 6). There is a north-south asymmetry, with a higher occurrence rate in the north, regardless of the upstream IMF polarity, as the twist in the tail topology is averaged out for each hemisphere. This north-south asymmetry probably occurs because (1) cusps of open field lines consist of a small spatial area/solid angle over the southern strong crustal fields such that the overall occurrence rate for open topology in the southern hemisphere is not necessarily higher than that in the northern hemisphere, except for right at the cusp regions at low altitudes; (2) more deeply draped field lines (into the collisional atmosphere) in the northern hemisphere are identified as open field lines by our technique; and (3) we



**Figure 6.** Occurrence rates of open topology in the  $X_{\text{MSO}} - R_{\text{MSO}}$  projection for all MAVEN data (left), east (middle), and west IMF (right), respectively. The white dashed lines are conic fits of the induced magnetic boundary from Vignes et al. (2000).



underestimate the occurrence rate of open field lines over strong crustal sources because of SWEA's limited ability to detect small loss cone angles. One noticeable difference is that the occurrence rate for  $R_{MSO} < 0$  and  $X < -1.5 R_M$  is higher for east IMF's (middle) than west IMF's (right). This difference mirrors the low occurrence rate of open topology in the south for west IMF's (the lower right of Figure 4), probably because of the different reconnection patterns for east and west IMF's, which likely results in different occurrence rates for open field lines. In addition, if west IMF's result in more connectivity to strong crustal sources than the reverse polarity, SWEA's limited ability to detect small loss cones may artificially suppress the observed occurrence rate of open field lines.

#### 4. Discussion and Conclusions

Motivated by the evidence that the apparent twist of the Martian magnetotail is caused by reconnection between the IMF and the crustal fields (DiBraccio et al., 2018), we compare magnetic topology inferred from the MAVEN data with that from MHD simulations. From both the model and data, Mars's magnetotail is found to be dominated by combinations of draped and open magnetic topologies, and not merely draped IMF's as at Venus. In addition, the pattern of open field lines in the tail at  $X = [-1.5, -3] R_M$  twists by  $\sim 90^\circ$  in response to reversing IMF polarity, in the same sense as the tail magnetic polarity pattern and cross-tail current sheet, as inferred by DiBraccio et al. These results are consistent with the interpretation that a large portion of open field lines populating the tail produces the twist.

The topology results from the model and data show significant differences, such as the absolute occurrence rates, for which a combination of caveats in the model results and/or data-derived topology products, as well as uncertainties in upstream clock angles, might be responsible. However, a detailed analysis to determine specifically what causes these differences could require time-dependent simulations, a better representation of magnetic reconnection in the models, and sampling the models along the MAVEN trajectory to recreate the data sampling function. Each of these tasks is beyond the scope of this study. Instead, the qualitative agreements on the gross features in the model and data results in this study have provided useful insights to the implication of topology being the cause of the twist in the tail, which varies significantly for different IMF polarities interacting with the crustal fields.

One might argue that magnetic topology inferred from superthermal electrons cannot distinguish deeply draped IMF below the electron exobase from field lines connected to the surface, so that some field lines identified as open by our technique may in fact be deeply draped. However, the variation in occurrence rates of open field lines in response to changes in the IMF polarity supports the interpretation that Mars's crustal magnetic fields cause the tail twist, because the conditions for magnetic reconnection between IMF and crustal magnetic fields depend on IMF polarity. These same conditions also affect where the draped IMF can penetrate deeply into the ionosphere. In other words, both open field lines connected to the surface and deeply draped field lines are affected by the interaction between crustal magnetic fields and IMF, which is why both types of "open" field lines can vary with upstream IMF polarities.

This tail topology variation with the IMF polarity also echoes draped field distortions revealed by Brain et al. (2006) with Mars Global Surveyor observations: the magnetic field at 400-km altitude over a northern weak crustal region is more consistent with a draping pattern under the west IMF but more scattered in directions under the east IMF. Luhmann et al. (2015b) showed from MHD simulations that this distortion is likely due to different reconnection geometries for different IMF polarities. While the results from Brain et al. (2006) are for dayside, open field lines from dayside magnetic reconnection will populate part of the tail lobes, forming at least part of the open-to-day topology seen in the tail. In all, previous studies and our results suggest that the Martian crustal magnetic fields have a global effect on the magnetosphere configuration, supporting the picture of a hybrid magnetotail at Mars.

#### Acknowledgments

The MAVEN project is supported by NASA through the Mars Exploration Program. The MAVEN data used in this study are available through Planetary Data System (<https://pds-ppi.igpp.ucla.edu/mission/MAVEN>). The BATS-R-US code is publicly available (<http://csem.engin.umich.edu/tools/swmf>). S. Xu gratefully acknowledges the artistic skills of Jessica Still and the time she dedicated to create the schematics presented in Figure 1.

#### References

- Acuna, M., Connerney, J., Lin, R., Mitchell, D., Carlson, C., McFadden, J., et al. (1999). Global distribution of crustal magnetization discovered by the Mars Global Surveyor MAG/ER experiment. *Science*, *284*(5415), 790–793.
- Adams, D., Xu, S., Mitchell, D. L., Lillis, R. L., Fillingim, M., Andersson, L., et al. (2018). Using magnetic topology to probe the sources of Mars' nightside ionosphere. *Geophysical Research Letters*, *45*, 12,190–12,197. <https://doi.org/10.1029/2018GL080629>
- Akbari, H., Andersson, L., Peterson, W., Espley, J., Benna, M., & Ergun, R. (2019). Ambipolar electric field in the Martian ionosphere: MAVEN measurements. *Journal of Geophysical Research: Space Physics*, *124*, 4518–4524. <https://doi.org/10.1029/2018JA026325>
- Bertucci, C., Duru, F., Edberg, N., Fraenz, M., Martinecz, C., Szego, K., & Vaisberg, O. (2011). The induced magnetospheres of Mars, Venus, and Titan. *Space Science Reviews*, *162*(1–4), 113–171.

- Brain, D., Lillis, R., Mitchell, D., Halekas, J., & Lin, R. (2007). Electron pitch angle distributions as indicators of magnetic field topology near Mars. *Journal of Geophysical Research*, *112*, A09201. <https://doi.org/10.1029/2007JA012435>
- Brain, D. A., Mitchell, D. L., & Halekas, J. S. (2006). The magnetic field draping direction at Mars from April 1999 through August 2004. *Icarus*, *182*(2), 464–473.
- Coates, A. J., Tsang, S., Wellbrock, A., Frahm, R., Winningham, J., Barabash, S., et al. (2011). Ionospheric photoelectrons: Comparing Venus, Earth, Mars and Titan. *Planetary and Space Science*, *59*(10), 1019–1027.
- Collinson, G., Mitchell, D., Glocer, A., Grebowsky, J., Peterson, W. K., Connerney, J., et al. (2015). Electric Mars: The first direct measurement of an upper limit for the Martian "polar wind" electric potential. *Geophysical Research Letters*, *42*, 9128–9134. <https://doi.org/10.1002/2015GL065084>
- Connerney, J., Acuña, M., Ness, N., Kletetschka, G., Mitchell, D., Lin, R., & Reme, H. (2005). Tectonic implications of Mars crustal magnetism. *Proceedings of the national Academy of Sciences of the United States of America*, *102*(42), 14,970–14,975.
- Connerney, J., Espley, J., Lawton, P., Murphy, S., Odom, J., Oliverson, R., & Sheppard, D. (2015). The MAVEN magnetic field investigation. *Space Science Reviews*, *195*, 257–291.
- Cowley, S. (1981). Magnetospheric asymmetries associated with the y-component of the IMF. *Planetary and Space Science*, *29*(1), 79–96.
- Cravens, T. E., Hamil, O., Houston, S., Bougher, S., Ma, Y., Brain, D., & Ledvina, S. (2017). Estimates of ionospheric transport and ion loss at Mars. *Journal of Geophysical Research: Space Physics*, *122*, 10,626–10,637. <https://doi.org/10.1002/2017JA024582>
- DiBraccio, G. A., Luhmann, J. G., Curry, S. M., Espley, J. R., Xu, S., Mitchell, D. L., et al. (2018). The twisted configuration of the Martian magnetotail: MAVEN observations. *Geophysical Research Letters*, *45*, 4559–4568. <https://doi.org/10.1029/2018GL077251>
- Dong, C., Bougher, S. W., Ma, Y., Toth, G., Nagy, A. F., & Najib, D. (2014). Solar wind interaction with Mars upper atmosphere: Results from the one-way coupling between the multifluid MHD model and the MTGCM model. *Geophysical Research Letters*, *41*, 2708–2715. <https://doi.org/10.1002/2014GL059515>
- Dong, Y., Fang, X., Brain, D., Hurley, D., Halekas, J., Espley, J., et al. (2019). Magnetic field in the Martian magnetosheath and the application as an IMF clock angle proxy. *Journal of Geophysical Research: Space Physics*, *124*, 4295–4313. <https://doi.org/10.1029/2019JA026522>
- Dubinin, E., & Fraenz, M. (2015). Magnetotails of Mars and Venus. *Magnetotails in the solar system* (Vol. 207, pp. 34–59). NJ: John Wiley Hoboken.
- Dubinin, E., Fraenz, M., Pätzold, M., McFadden, J., Halekas, J., DiBraccio, G., et al. (2017). The effect of solar wind variations on the escape of oxygen ions from Mars through different channels: MAVEN observations. *Journal of Geophysical Research: Space Physics*, *122*, 11,285–11,301. <https://doi.org/10.1002/2017JA024741>
- Dubinin, E. M., Izrailevich, P., & Podgorny, I. (1980). The combined magnetosphere. *Kosmicheskie Issledovaniia*, *18*, 470–474.
- Dubinin, E., Lundin, R., & Schwingenschuh, K. (1994). Solar wind electrons as tracers of the Martian magnetotail topology. *Journal of Geophysical Research*, *99*(A11), 21,233–21,240.
- Ergun, R. E., Andersson, L. A., Fowler, C. M., Woodson, A. K., Weber, T. D., Delory, G. T., et al. (2016). Enhanced  $O_2^+$  loss at Mars due to an ambipolar electric field from electron heating. *Journal of Geophysical Research: Space Physics*, *121*, 4668–4678. <https://doi.org/10.1002/2016JA022349>
- Ergun, R. E., Morooka, M. W., Andersson, L. A., Fowler, C. M., Delory, G. T., Andrews, D. J., et al. (2015). Dayside electron temperature and density profiles at Mars: First results from the MAVEN Langmuir probe and waves instrument. *Geophysical Research Letters*, *42*, 8846–8853. <https://doi.org/10.1002/2015GL065280>
- Fang, X., Liemohn, M. W., Nagy, A. F., Ma, Y., De Zeeuw, D. L., Kozyra, J. U., & Zurbuchen, T. H. (2008). Pickup oxygen ion velocity space and spatial distribution around Mars. *Journal of Geophysical Research*, *113*, A02210. <https://doi.org/10.1029/2007JA012736>
- Fillingim, M. O., Peticolas, L. M., Lillis, R. J., Brain, D. A., Halekas, J. S., Mitchell, D. L., et al. (2007). Model calculations of electron precipitation induced ionization patches on the nightside of Mars. *Geophysical Research Letters*, *34*, L12101. <https://doi.org/10.1029/2007GL029986>
- Frahm, R., Sharber, J., Winningham, J., Link, R., Liemohn, M., Kozyra, J., et al. (2010). Estimation of the escape of photoelectrons from Mars in 2004 liberated by the ionization of carbon dioxide and atomic oxygen. *Icarus*, *206*(1), 50–63.
- Frahm, R., Sharber, J., Winningham, J., Wurz, P., Liemohn, M., Kallio, E., et al. (2006). Locations of atmospheric photoelectron energy peaks within the Mars environment. *Space Science Reviews*, *126*(1–4), 389–402.
- Fränz, M., Dubinin, E., Andrews, D., Barabash, S., Nilsson, H., & Fedorov, A. (2015). Cold ion escape from the Martian ionosphere. *Planetary and Space Science*, *119*, 92–102.
- Halekas, J., Brain, D., Luhmann, J., DiBraccio, G., Ruhunusiri, S., Harada, Y., et al. (2017a). Flows, fields, and forces in the Mars-solar wind interaction. *Journal of Geophysical Research: Space Physics*, *122*, 11,320–11,341. <https://doi.org/10.1002/2017JA024772>
- Halekas, J., Ruhunusiri, S., Harada, Y., Collinson, G., Mitchell, D., Mazelle, C., et al. (2017b). Structure, dynamics, and seasonal variability of the Mars-solar wind interaction: MAVEN solar wind ion analyzer in-flight performance and science results. *Journal of Geophysical Research: Space Physics*, *122*, 547–578. <https://doi.org/10.1002/2016JA023167>
- Halekas, J., Taylor, E., Dalton, G., Johnson, G., Curtis, D., McFadden, J., et al. (2015). The solar wind ion analyzer for MAVEN. *Space Science Reviews*, *195*(1–4), 125–151.
- Harada, Y., Halekas, J. S., DiBraccio, G. A., Xu, S., Espley, J., McFadden, J. P., et al. (2018). Magnetic reconnection on dayside crustal magnetic fields at Mars: MAVEN observations. *Geophysical Research Letters*, *45*, 4550–4558. <https://doi.org/10.1002/2018GL077281>
- Harada, Y., Halekas, J., McFadden, J., Espley, J., DiBraccio, G., Mitchell, D., et al. (2017). Survey of magnetic reconnection signatures in the Martian magnetotail with MAVEN. *Journal of Geophysical Research: Space Physics*, *122*, 5114–5131. <https://doi.org/10.1002/2017JA023952>
- Inui, S., Seki, K., Sakai, S., Brain, D., Hara, T., McFadden, J., et al. (2018). Statistical study of heavy ion outflows from Mars observed in the Martian-induced magnetotail by MAVEN. *Journal of Geophysical Research: Space Physics*, *124*, 5482–5497. <https://doi.org/10.1029/2018JA026452>
- Jakosky, B., Brain, D., Chaffin, M., Curry, S., Deighan, J., Grebowsky, J., et al. (2018). Loss of the Martian atmosphere to space: Present-day loss rates determined from MAVEN observations and integrated loss through time. *Icarus*, *315*, 146–157. <https://doi.org/10.1016/j.icarus.2018.05.030>
- Liemohn, M. W., Ma, Y., Frahm, R. A., Fang, X., Kozyra, J. U., Nagy, A. F., et al. (2006). Mars global MHD predictions of magnetic connectivity between the dayside ionosphere and the magnetospheric flanks. *Space Science Reviews*, *126*, 63–76. <https://doi.org/10.1007/s11214-006-9116-8>
- Liemohn, M. W., & Xu, S. (2018). Recent advances regarding the Mars magnetotail current sheet. *Electric Currents in Geospace and Beyond*, *235*, 177.
- Lillis, R. J., & Brain, D. A. (2013). Nightside electron precipitation at Mars: Geographic variability and dependence on solar wind conditions. *Journal of Geophysical Research: Space Physics*, *118*, 3546–3556. <https://doi.org/10.1002/jgra.50171>

- Lillis, R. J., Fillingim, M. O., & Brain, D. A. (2011). Three-dimensional structure of the Martian nightside ionosphere: Predicted rates of impact ionization from Mars Global Surveyor magnetometer and electron reflectometer measurements of precipitating electrons. *Journal of Geophysical Research*, *116*, A12317. <https://doi.org/10.1029/2011JA016982>
- Luhmann, J. (1986). The solar wind interaction with Venus. *Space science reviews*, *44*(3-4), 241–306.
- Luhmann, J., Dong, C., Ma, Y., Curry, S., Mitchell, D., Espley, J., et al. (2015a). Implications of MAVEN Mars near-wake measurements and models. *Geophysical Research Letters*, *42*, 9087–9094. <https://doi.org/10.1002/2015GL066122>
- Luhmann, J., Ma, Y.-J., Brain, D., Ulusen, D., Lillis, R., Halekas, J., & Espley, J. (2015b). Solar wind interaction effects on the magnetic fields around Mars: Consequences for interplanetary and crustal field measurements. *Planetary and Space Science*, *117*, 15–23.
- Ma, Y., Fang, X., Russell, C. T., Nagy, A. F., Toth, G., Luhmann, J. G., et al. (2014). Effects of crustal field rotation on the solar wind plasma interaction with Mars. *Geophysical Research Letters*, *41*, 6563–6569. <https://doi.org/10.1002/2014GL060785>
- Ma, Y., Nagy, A. F., Hansen, K. C., DeZeeuw, D. L., Gombosi, T. I., & Powell, K. (2002). Three-dimensional multispecies MHD studies of the solar wind interaction with Mars in the presence of crustal fields. *Journal of Geophysical Research*, *107*(A10), 1282–1289.
- Ma, Y., Nagy, A. F., Sokolov, I. V., & Hansen, K. C. (2004). Three-dimensional, multispecies, high spatial resolution MHD studies of the solar wind interaction with Mars. *Journal of Geophysical Research*, *109*, A07211. <https://doi.org/10.1029/2003JA010367>
- McComas, D. J., Spence, H. E., Russell, C., & Saunders, M. (1986). The average magnetic field draping and consistent plasma properties of the Venus magnetotail. *Journal of Geophysical Research*, *91*(A7), 7939–7953.
- Mitchell, D., Lin, R., Mazelle, C., Reme, H., Cloutier, P., Connerney, J., et al. (2001). Probing Mars' crustal magnetic field and ionosphere with the MGS electron reflectometer. *Journal of Geophysical Research*, *106*(E10), 23,419–23,427.
- Mitchell, D., Mazelle, C., Sauvaud, J.-A., Thocaven, J.-J., Rouzaud, J., Fedorov, A., et al. (2016). The MAVEN solar wind electron analyzer. *Space Science Reviews*, *200*(1-4), 495–528.
- Némeç, F., Morgan, D. D., Gurnett, D. A., & Duru, F. (2010). Nightside ionosphere of Mars: Radar soundings by the Mars Express spacecraft. *Journal of Geophysical Research*, *115*, E12009. <https://doi.org/10.1029/2010JE003663>
- Nagy, A., Winterhalter, D., Sauer, K., Cravens, T., Brecht, S., Mazelle, C., et al. (2004). The plasma environment of Mars, *Mars? Magnetism and Its Interaction with the Solar Wind* (pp. 33–114): Springer.
- Phillips, J., & Russell, C. (1987). Revised upper limit on the internal magnetic moment of Venus. *Advances in Space Research*, *7*(12), 291–294.
- Saunders, M., & Russell, C. (1986). Average dimension and magnetic structure of the distant Venus magnetotail. *Journal of Geophysical Research*, *91*(A5), 5589–5604.
- Shane, A. D., Xu, S., Liemohn, M. W., & Mitchell, D. L. (2016). Mars nightside electrons over strong crustal fields. *Journal of Geophysical Research: Space Physics*, *121*, 3808–3823. <https://doi.org/10.1002/2015JA021947>
- Steckiewicz, M., Mazelle, C., Garnier, P., André, N., Penou, E., Beth, A., et al. (2015). Altitude dependence of nightside Martian suprathermal electron depletions as revealed by MAVEN observations. *Geophysical Research Letters*, *42*, 8877–8884. <https://doi.org/10.1002/2015GL065257>
- Vignes, D., Mazelle, C., Rme, H., Acuña, M. H., Connerney, J. E. P., Lin, R. P., et al. (2000). The solar wind interaction with Mars: Locations and shapes of the bow shock and the magnetic pile-up boundary from the observations of the MAG/ER experiment onboard Mars Global Surveyor. *Geophysical Research Letters*, *27*, 49–52. <https://doi.org/10.1029/1999GL010703>
- Weber, T., Brain, D., Mitchell, D., Xu, S., Connerney, J., & Halekas, J. (2017). Characterization of low-altitude nightside Martian magnetic topology using electron pitch angle distributions. *Journal of Geophysical Research: Space Physics*, *122*, 9777–9789. <https://doi.org/10.1002/2017JA024491>
- Weber, T., Brain, D., Mitchell, D., Xu, S., Espley, J., Halekas, J., et al. (2019). The influence of solar wind pressure on Martian crustal magnetic field topology. *Geophysical Research Letters*, *46*, 2347–2354. <https://doi.org/10.1029/2019GL081913>
- Xu, S., Curry, S. M., Mitchell, D. L., Luhmann, J. G., Lillis, R. J., & Dong, C. (2019a). Magnetic topology response to the 2003 halloween ICME event at Mars. *Journal of Geophysical Research: Space Physics*, *124*, 151–165. <https://doi.org/10.1029/2018JA026118>
- Xu, S., Fang, X., Mitchell, D. L., Ma, Y., Luhmann, J. G., DiBraccio, G. A., et al. (2018a). Investigation of Martian magnetic topology response to 2017 September ICME. *Geophysical Research Letters*, *45*, 7337–7346. <https://doi.org/10.1029/2018GL077708>
- Xu, S., Liemohn, M., Bougher, S., & Mitchell, D. (2016b). Martian high-altitude photoelectrons independent of solar zenith angle. *Journal of Geophysical Research: Space Physics*, *121*, 3767–3780. <https://doi.org/10.1002/2015JA022149>
- Xu, S., Mitchell, D., Liemohn, M., Dong, C., Bougher, S., Fillingim, M., et al. (2016a). Deep nightside photoelectron observations by MAVEN SWEA: Implications for Martian northern hemispheric magnetic topology and nightside ionosphere source. *Geophysical Research Letters*, *43*, 8876–8884. <https://doi.org/10.1002/2016GL070527>
- Xu, S., Mitchell, D., Liemohn, M., Fang, X., Ma, Y., Luhmann, J., et al. (2017a). Martian low-altitude magnetic topology deduced from MAVEN/SWEA observations. *Journal of Geophysical Research: Space Physics*, *122*, 1831–1852. <https://doi.org/10.1002/2016JA023467>
- Xu, S., Mitchell, D., Luhmann, J., Ma, Y., Fang, X., Harada, Y., et al. (2017b). High-altitude closed magnetic loops at Mars observed by MAVEN. *Geophysical Research Letters*, *44*, 11,229–11,238. <https://doi.org/10.1002/2017GL075831>
- Xu, S., Mitchell, D. L., McFadden, J. P., Collinson, G., Harada, Y., Lillis, R., et al. (2018b). Field-aligned potentials at Mars from MAVEN observations. *Geophysical Research Letters*, *45*, 10,119–10,127. <https://doi.org/10.1029/2018GL080136>
- Xu, S., Weber, T., Mitchell, D. L., Brain, D. A., Mazelle, C., DiBraccio, G. A., & Espley, J. (2019b). A technique to infer magnetic topology at Mars and its application to the terminator region. *Journal of Geophysical Research: Space Physics*, *124*, 1823–1842. <https://doi.org/10.1029/2018JA026366>
- Zhang, T., Baumjohann, W., Du, J., Nakamura, R., Jarvinen, R., Kallio, E., et al. (2010). Hemispheric asymmetry of the magnetic field wrapping pattern in the Venusian magnetotail. *Geophysical Research Letters*, *37*, L14202. <https://doi.org/10.1029/2010GL044020>